Karkowska and Wilde-Piórko
Earth, Planets and Space (2022) 74:150
https://doi.org/10.1186/s40623-022-01712-4

Earth, Planets and Space

FULL PAPER

Determination of the Earth's structure based on intermediate-period surface wave recordings of tidal gravimeters: a case study

Kamila Karkowska[1,2*] and Monika Wilde-Piórko[1]

Abstract

Tidal gravimeters can detect intermediate-period surface waves with high accuracy. Three gravimetric stations with estimated transfer functions and co-located with seismic stations were selected: two in Belgium (Membach and Rochefort, in Western Europe) and one in Germany (Black Forest, in Central Europe). The compatibility of gravimetric and seismic recordings of earthquakes in the period range of 10-180 s has been presented. The series of monochromatic signals separated from surface waves for selected events have been calculated using the multiple-filtering procedure, and averaged fundamental-mode Rayleigh wave group-velocity curves have been estimated on a regional scale. Next, averaged dispersion curves for three regions (Italy, Greece, and Western Turkey) were inverted by weighted linear inversion methods. Additionally, a quantitative analysis of resolution tests of inverted models was presented to show the capabilities of the gravimetric data to retrieve a shear-wave velocity distribution with a depth. In particular, a method for determining the depth range of the inverted model has been proposed. Results obtained based on gravimetric data were verified by results from seismic data obtained by applying the same procedure. This study shows the novel application of tidal gravimetric data in the determination of the regional Earth's structure based on intermediate-period surface waves recordings, as well as a comprehensive approach to the quantitative estimation of a final model resolution.

Keywords: Rayleigh waves dispersion curves, Linear inversion, Tidal gravimeters, BB seismometers

*Correspondence: kamila.karkowska@igik.edu.pl

[1] Centre of Geodesy and Geodynamics, Institute of Geodesy and Cartography, Z. Modzelewskiego St. 27, 02-679 Warsaw, Poland
Full list of author information is available at the end of the article

Graphical Abstract

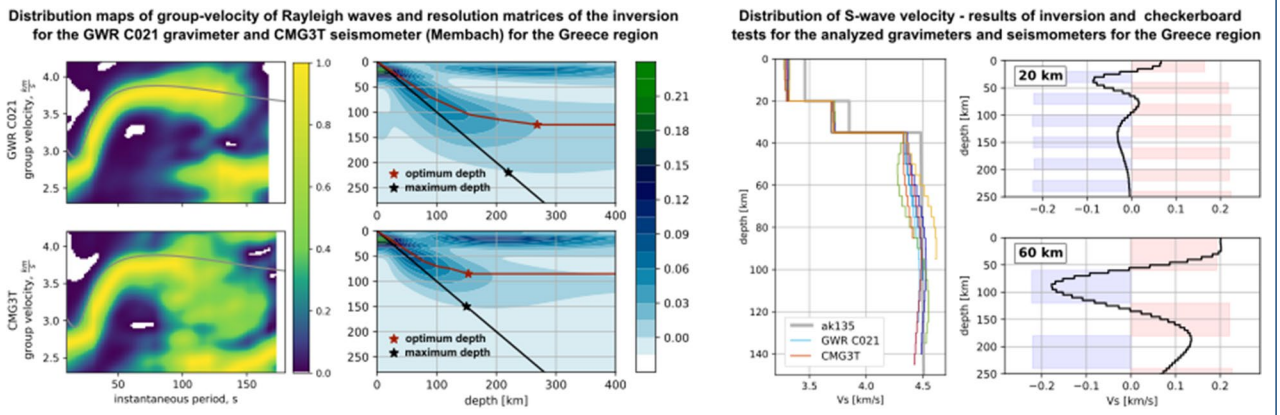

Introduction

A gravimeter, just like a seismometer, is an inertial sensor that is sensitive to acceleration. The wide range of frequencies which are recorded by tidal gravimeters allows to use them not only for analysing tidal effects but also for monitoring short and very short-term phenomena. In the twentieth century, gravimetric recordings were typically used to analyse Earth's free oscillations. Nowadays, the most precise tidal gravimeters. i.e. superconducting gravimeters, can monitor many effects, such as hydrogeological, hydrothermal, post-seismic and post-glacial relaxation or volcanic ones (Van Camp et al. 2017).

The performance of tidal gravimeters in a seismic frequency band has been tested by e.g. Freybourger et al. (1997); Banka & Crossley (1999); Rosat et al. (2004), and Forbriger et al. (2021), based on the analysis of the power spectral density of noise level of those instruments. Also, seismic normal modes recorded by the tidal gravimeters after largest earthquakes were analysed by, e.g. Richter et al. (1995); Freybourger et al. (1997); Van Camp (1999), and Rosat et al. (2005). Recently, recordings of globally distributed superconducting gravimeters have been analysed by Li et al. (2020) for the estimation of long-period surface waves and free oscillations using an autocorrelation ambient-noise technique. These studies have proven that gravimetric recordings are indispensable for research in the normal mode of seismic waves and Earth's free oscillation frequency band.

A comprehensive approach to earthquake records made by a tidal gravimeter has been presented by Karkowska et al. (2022). In total, over 10,000 traces of worldwide earthquakes from 2013-2020 were investigated to show that recordings of earthquakes in the period range of 10–1000 s performed by tidal gravimeters and broadband seismometers correspond very well to each other in the period ranges of instruments' operability. A simple processing scheme of the gravimetric signal of earthquakes, taking into account a transfer function of each instrument, was proposed, and global group-velocity dispersion curves of the fundamental mode of Rayleigh waves were estimated up to the period of 500 s. However, no detailed studies have been carried out on analysing the regional distribution of group-velocity of surface waves.

A detailed analysis of surface wave data and methods used for identifying and measuring signal parameters was presented by Levshin et al. (1989), and a concise overview of the progress made in the last few decades in the determination of the Earth structure based on these data was given by Romanowicz (2002). Bormann et al. (2012) noted that, when inverting a surface wave dispersion curve up to 500 s, it is possible to retrieve information on the shear-wave velocity (V_s) structure of the upper mantle and the transition zone up to the lower mantle. However, the typically analysed maximum period of surface waves recorded by broadband seismometers is 100–180 s (e.g. Stehly et al. 2009; Chrapkiewicz et al. 2020). A resolving power of a given inversion scheme can be estimated based on the resolution matrix whenever possible (e.g. Gubbins 2004). Typically, a depth range of a model inverted based on dispersion curves of surface waves is determined from the maximum peak (Verbeke et al. 2012) or the range of maximum sensitivity of surface wave velocities in depths (e.g. Stehly et al. 2009). Additionally, checkerboard recovery tests are routinely performed to estimate a reliability of applied inversion scheme, in particular to examine the observed spatial lateral

heterogeneities of surface wave velocities (e.g. Li et al. 2010; Verbeke et al. 2012). Chrapkiewicz et al. (2020) have proposed to adopt a checkerboard test to 1D problem to tackle the credibility of the final model of the distribution of V_s with depths, inverted based on a velocity dispersion curve of the surface wave.

This paper presents the novel concept of using tidal gravimetric recordings to improve the determination of the regional Earth's structure by measuring and inversion of the dispersion curve of Rayleigh surface waves of intermediate periods, i.e. 10–180 s. Such studies have not been performed yet. Time series from tidal gravimeters and co-located broadband seismometers (only vertical component) from Central Europe will be analysed. Appropriate pre-processing of gravimetric data, including the deconvolution of the gravimeter transfer function, will be proposed. Group velocities of fundamental-mode of Rayleigh waves recorded by the tidal gravimeters and co-located seismometers will be measured, and the linear inversion algorithm will be applied to retrieve S-wave velocity models for Central and Southern Europe. Additionally, the comprehensive evaluation of accuracy of resulted models by quantitative analysis of resolution matrices and checkerboard test will be presented to show that gravimetric recordings can complement the seismic ones in regional determinations of the Earth's crustal and mantle structure.

Data

Selection criteria

Three data selection criteria are considered: (1) co-location of gravimeter and seismometer sensors; (2) the accessibility of 1-Hz raw gravimetric data (necessary to compare the gravimetric and seismic recordings of earthquakes in the period range of 10–180 s); (3) the availability of gravimeter's transfer function. Finally, only three stations fulfil all criteria: one located in Germany (Central Europe): Black Forest (BFO), and two in Belgium (Western Europe): Membach (MEM) and Rochefort (RCHB). Selected observatories upload both gravimetric and seismic recordings to the IRIS database, which facilitates the process of downloading data and instrument's transfer function (http://ds.iris.edu/ds/nodes/dmc/data/types/waveform-data/, last accessed 4 January 2021). Each selected station provides data recorded by a superconducting gravimeter (SG) and a very broadband (VBB) or broadband (BB) seismometer. The Black Forest Observatory also supplies data from the spring gravimeter LaCoste and Romberg (LCR) ET-19. Table 1 presents a summary of sensors type and periods of analysed data.

The compatibility of gravimetric and seismic data in the intermediate seismic frequency band, i.e. in the period range of 10–180 s, is tested based on recordings of events from three regions: Italy, Greece, and Western Turkey. The quality of recordings of earthquakes is checked automatically based on the signal-to-noise ratio. Then, based on manual verification of gravimetric recordings, the final list of events with visible seismic energy is created. The magnitudes of events are in the range of $3.0 - 6.6$. Location of stations, number of considered earthquakes, and distribution of their epicentres divided into regions mentioned above together with a simplified geological map of analysed regions and their surroundings (Pawlewicz et al. 2002) are shown in Fig. 1.

Data pre-processing

The scheme of data pre-processing is similar for both gravimetric and seismic data, namely (1) selection of the event window based on the EMSC bulletin; (2) removal of the instrument response (transfer function) together with detrending, tapering, filtering, and differentiating of the signal; the last process applied only for seismic data to prepare waveforms from all instruments in units of acceleration consistently); (3) application of the zero-phase 4th-order bandpass Butterworth filter with corner frequencies of 10 and 180s; (4) resampling of seismic data to 1Hz (frequency of gravimetric data). The consideration of the transfer function of the instrument plays a

Table 1 List of instruments (gravimeters and seismometers) together with the period of analysed data and site coordinates

Seismic station's code	Period of analysed data	Gravimeter	Seismometer	Coordinates	
				Latitude [degrees]	Longitude [degrees]
BFO	07.2013–09.2019	GWR SG-056 L LCR ET19	STS-1 (VBB)	48.3301	8.3296
MEM	01.2006–09.2019	GWR C021	CMG3T 30s (BB)	50.6092	6.0067
RCHB	06.2017–09.2019	GWR iGrav 019	Trillium Compact 120s (BB)	50.1552	5.2260

All data were downloaded from the IRIS database

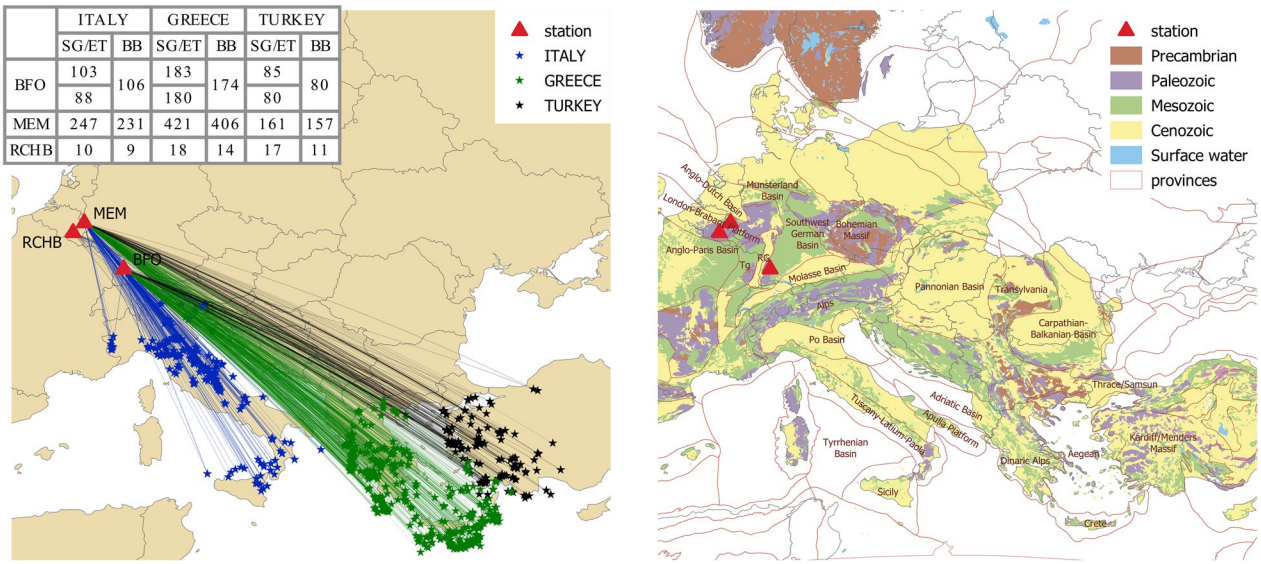

Fig. 1 Distribution of epicentres of earthquakes used in the regional scale analysis of group-velocity dispersion curves of Rayleigh waves together with great circles of waves propagation (left) and simplified geological map (Pawlewicz et al. 2002) of analysed regions and their surroundings (right). Codes of stations refer to seismic stations; in the left upper corner a summary of the number of events considered for particular regions is shown; *RG* Rhine Graben, *Tg* Trans-graben

vital role in the processing of intermediate-period surface wave recordings. Detailed analysis of the transfer function of seismometer and gravimeter in the period range of 10–1000 s for instruments from the Black Forest, Membach and Rochefort stations, as well as justification of the data processing scheme applied, are presented in Karkowska et al. (2022). Filtering in the range of 2-1000 s has been also tested. It resulted however, in numerical noise amplification between 0.3 and 0.5 Hz in the case of the Black Forest gravimeter due to the instrument's transfer function. In order to standardise the data processing scheme for all stations, waveforms are filtered in the range of 10-1000 s.

The example of pre-processed recordings of Greece earthquake from the Membach station is shown in Fig. 2. The coefficient of correlation between seismic and gravimetric data of 0.987, calculated separately for the whole recording and the surface waves only, which shows an excellent consistency between seismic and gravimetric recordings.

Methodology

Gaussian filtering

The procedure described by Kolínský (2004) is followed to calculate individual group-velocity dispersion curves. Non-constant relative resolution filtering with the filter coefficient linearly dependent on a period (Dziewonski et al. 1969; Kolínský 2004) is applied in the multiple-filtering procedure. One hundred Gaussian filters of central periods in the range of 10–180 s are considered. Finally, to construct dispersion curves for all events the instantaneous periods are calculated (Lander 1989) and used instead of central periods because of the asymmetric spectrum of the signals.

Figure 3 shows the example of the Greece earthquake wave trains recorded at the Black Forest and Membach stations. Wave trains of gravimetric and seismic signals match very well at the Black Forest station (GWR SG-056 L and VBB STS-1 seismometer). Such good compliance is not observed for the Membach station (GWR C021 and BB CMG3T seismometer), especially for periods larger than 70 s, because of 30 s CMG3T cut-off period.

Probability density distribution maps

All estimated individual dispersion curves are used to create probability density distribution maps. The examples of distribution maps for the Membach station instruments (all regions) are shown in Fig. 4. The yellow colour indicates the high probability (above 0.9) of group-velocity values at a given period. As a reference, the dispersion curve calculated for the 1-D ak135 velocity model (Kennett et al. 1995) is presented (solid grey line). Although the shape of the ridges of the most probable values are similar to the ak135 dispersion curve for periods up to about 100 s, lower values

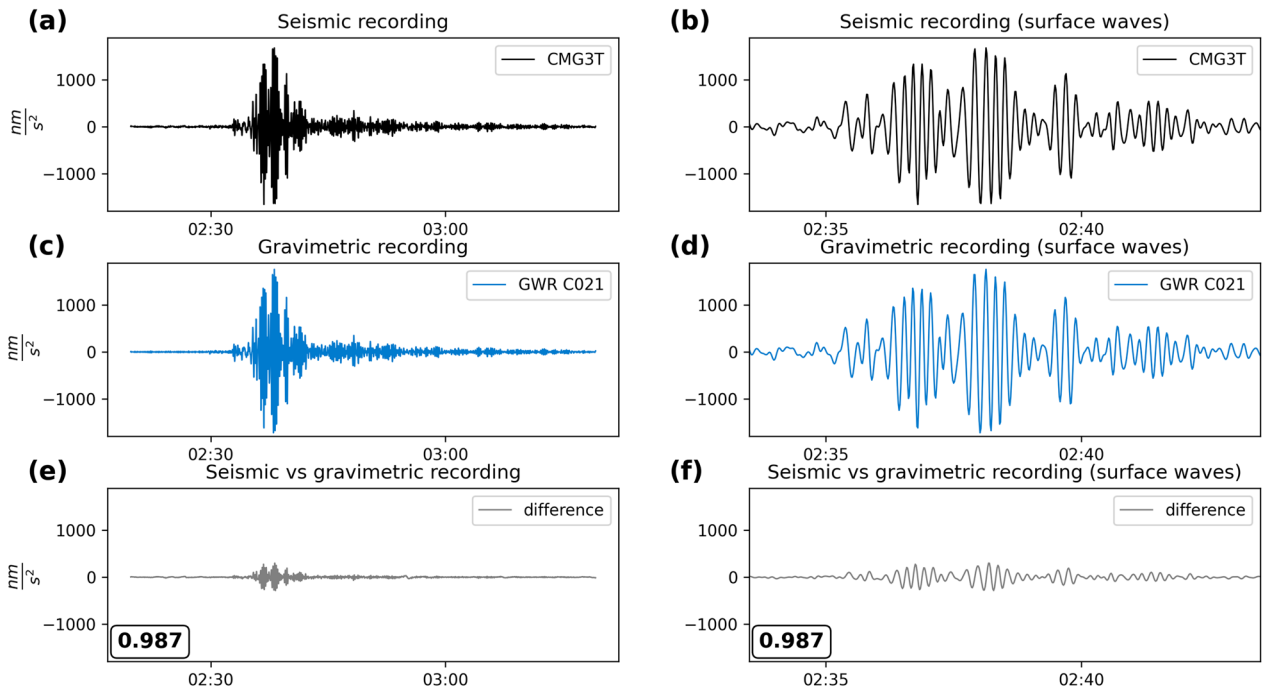

Fig. 2 Gravimetric vs seismic recordings of the M5.4 Greece earthquake (2019-02-05 02:26:09.4 UTC, 39.02°N, 20.56°E, depth 10km). On the left-hand side **a**, **c**, **e** full gravimetric (blue) and seismic (black) recordings of the earthquake from the Membach station and on the right-hand side (**b**, **d**, **f**) only surface waves are presented. In the left bottom corners, the parameter of correlation between seismic and gravimetric data are shown together with signal differences (subfigures **e**, **f**)

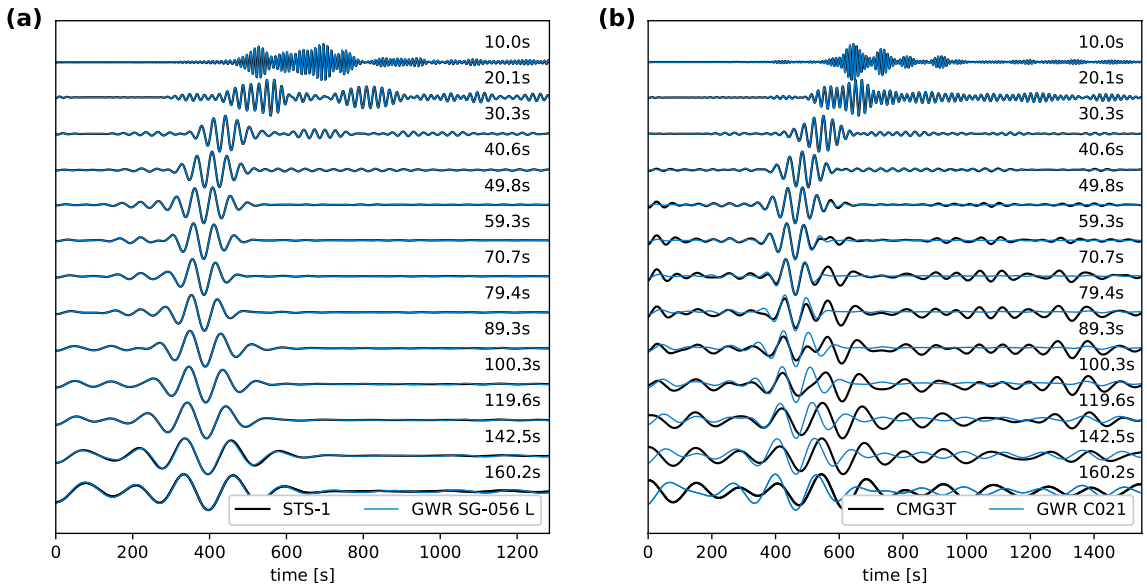

Fig. 3 Wave trains of the M5.4 Greece earthquake (2019-02-05 02:26:09.4 UTC, 39.02°N, 20.56°E, depth 10km) recorded by the SG (blue lines) and the co-located VBB and BB seismometers (black lines) of the Black Forest **a** and Membach **b** stations, respectively. Central periods are shown on the right for selected Gaussian filters

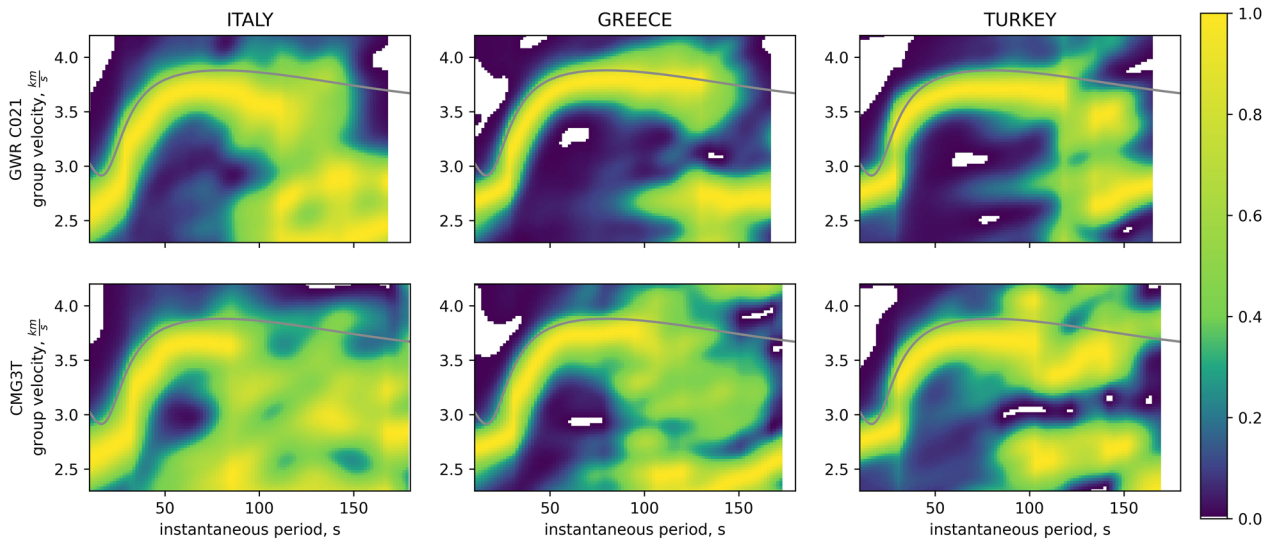

Fig. 4 Distribution maps of group-velocity of fundamental-mode Rayleigh waves for SG and BB of the Membach station calculated based on the Italy, Greece and Western Turkey earthquakes; the dispersion curve for the ak135 background model is shown as a solid grey line

by about 0.2–0.3 km/s can be observed for all regions. Distribution maps for all stations and regions are presented in (Additional file 1: Fig. S1).

Automatic selection of group-velocity dispersion curves of Rayleigh waves

The 1-D ak135 velocity model (background model) is used to validate measured individual dispersion curves. Automatic selection of calculated group-velocity values is performed based on two criteria described by Soomro et al. (2016). The first criterion is a background model criterion, defined by the difference between the estimated group-velocity and the value from the background model for each angular frequency. In this study, the threshold value (relative change) is set to 15% and is larger than the one used by Karkowska et al. (2022). In the beginning, several values of the threshold have been tested: 0.1, 0.15, 0.20, 0.25, and 0.3. The final threshold value is chosen based on compliance testings of the selected dispersion curves with the most probable dispersion curve estimated from the probability density distribution map for each instrument and each region. The second criterion is based on smoothness calculation, i.e. summed normalised difference of the first derivative of the measured and background values in the assumed angular frequency range. In this study, the threshold (the sum value) is set to 50s. Such a low value, more 'strict' compared to Karkowska et al. (2022), is adopted because of relatively scattered group-velocity values for a shorter period observed in the regional studies. Consequently, a more 'strict' criterion is necessary to obtain a good-quality estimation of averaged group-velocity dispersion curves of Rayleigh waves.

Averaged group-velocity dispersion curves of Rayleigh waves

The averaged dispersion curve is estimated as the mean value of group-velocities for each period (together with its standard deviation) from the automatically selected individual group-velocity dispersion curves of the Black Forest, Membach and Rochefort stations for three regions: Greece, Italy and Western Turkey (Fig. 5).

Ritzwoller & Levshin (1998) showed that the reliability of calculation of group-velocity curves degrades sharply below 20 s for regional distances. The presented study also confirms that finding, so dispersion measurements below 20 s is omitted. Bensen et al. (2007) recommended dispersion measurements only up to a cut-off period (in seconds) of about $\Delta/12$, where Δ is the distance between the station and the epicentre in km. The mean distance between the Black Forest station and epicentres of earthquakes from Italy is about 770 km, and for the Membach station—about 1030 km. Consequently, the recommended cut-off period is about 64 s, and 85 s for the Black Forest and Membach stations, respectively. The maximum distance between the Black Forest, and the epicentres of earthquakes from Western Turkey is about 1300 km and about 1630 km in the case of the Membach station, what results in the recommended cut-off period of 108 s, and 135 s, respectively. In this study, the range of periods is chosen for each instrument and region from the comparison of averaged dispersion curves calculated

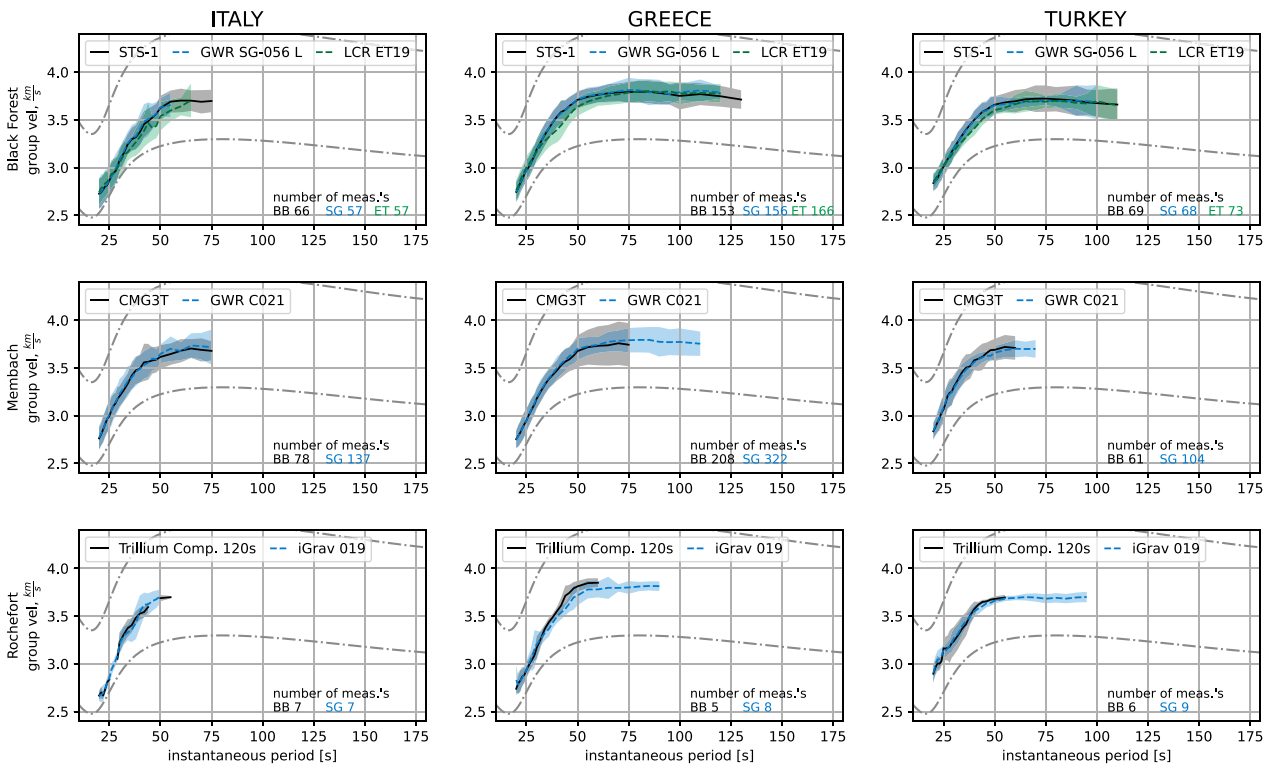

Fig. 5 Averaged dispersion curves of group-velocity of fundamental-mode Rayleigh waves (solid and dashed lines) with the standard deviation of individual measurements (shaded areas) and minimum and maximum value of the background model (dash-dotted grey lines) for each instrument of the Black Forest, Membach and Rochefort stations calculated for the Italy, Greece and Western Turkey regions, respectively

for all tested thresholds of the background model criterion. The minimum and maximum periods are estimated based on the criterion of the stable solution—for each period group-velocity values should converge to the same value, regardless of the threshold value.

The final number of measurements used to calculate averaged group-velocity dispersion curves are reduced by the usage of the automated selection method. The number of earthquakes used for estimating each instrument's average dispersion curve is presented in Fig. 5 in the right bottom corner of the subfigures. Notably, for the Membach station there is a substantial difference in the number of used individual dispersion curves calculated from the gravimetric and seismometric data. The CMG3T seismometer, which has the cut-off period of 30 s, caused a high attenuation of energy of waves of longer periods, so it provides data for the analysis of strong earthquakes only. Additionally, as a consequence, the standard deviations of individual seismic measurements for periods over $50-70$s are larger. The number of analysed earthquakes for the SG (GWR SG-056 L) and VBB (STS-1) at the Black Forest station are highly consistent for each region thanks to the similar registration ability of these instruments in the analysed period range. The time frame of analysed data for the Rochefort station is about two years which is relatively short compared to 6 and 13 years for the Black Forest and Membach stations, respectively. Consequently, the number of recorded events is low and it results in poor quality of the estimated averaged dispersion curves for the Rochefort station.

The presented results show an excellent consistency between averaged dispersion curves estimated from the data of tidal gravimeters and VBB and BB seismometers for each station and region. The only exception is the ET-19 spring gravimeter from the Black Forest station. The group-velocities of the ET-19 measured in the period range of 30–60 s exhibit lower values compared to those of SG and BB measurements (Fig. 5, top row). Amplitudes and phases of the ET-19's transfer function in this period range show some distortion, what could explain the observed deviation in averaged dispersion curves.

Estimated group-velocity dispersion curves of Rayleigh waves for selected regions are also in a very good agreement with the results of previous studies. Du et al. (1998) presented as an example a group-velocity dispersion curve of Rayleigh waves determined from 15 June 1995 Greece earthquake recorded by the CLZ seismic station in Central Germany to confront their model with

observed data. The measured velocities of 2.7 km/s for 20 s and 3.7 km/s for 100 s were just like those estimated in this study for the Membach and Black Forest stations from the Greece earthquakes (Fig. 5). Also, 2-D maps of Rayleigh group-velocity calculated by ambient-noise techniques have shown that averaged group-velocities up to the period of 40–50 s were much lower for the Italy paths than for the Greece or Western Turkey paths, while for longer periods, above 75 s, the larger velocities were observed along the Greece paths (e.g. Stehly et al. 2009; Verbeke et al. 2012; Lu et al. 2018).

Results and discussion

Linear inversion results and sensitivity kernels

Inversion aims to search for the best model of the Earth structure, whose forward response fits the experimental dispersion curves. Results are obtained using the iterative procedure started from the initial model, which is progressively adjusted by minimising the misfit function. The assumption is made that the 1-D model of the subsurface is constituted of a stack of homogeneous elastic layers. In the local search method used in this study, the initial model may have a significant impact on the result, so the choice of such model is crucial. Moreover, due to the assumption of linear inversion, the initial model should be close to the true structure. The ak135 model that fulfils the above requirements was chosen as the initial model down to the depth of 500 km (consists of layers of 5 km thick), below the sensitivity depth of Rayleigh waves of considered maximum periods. Differential smoothing of velocities between the adjacent layers is implemented in order to stabilise an underdetermined problem. Details about the used inversion scheme applied are presented by Herrmann and Ammon (2004).

The linear inversion method is applied to averaged group-velocity dispersion curves of Rayleigh waves for the Black Forest, Membach and Rochefort stations for three selected regions: Italy, Greece, and Western Turkey, respectively, to test the ability of the measured dispersion curves to find structure differences based on the gravimetric and seismic data. All results of linear inversion are presented in Fig. 6a–c. There is a visible decrease of S-wave velocities in the Earth's crust for all regions compared to the starting ak135 model. The sensitivity of the considered dispersion curves does not allow to retrieve the depths of the inter-crustal and the Moho discontinuities. Therefore, these boundary depths are reproduced from the starting ak135 model.

The sensitivity kernels are also calculated to estimate the relationship between the Earth's structure and dispersion velocities. Partial derivatives of the dispersion group-velocity (δU) with respect to the shear-wave (S) velocity (δV_s) calculated for periods of 20, 40, 60, 80, 100, and 120 s are presented in Fig. 6d. Because the resulted models are quite similar to each other and the shape of sensitivity kernels depends mainly on periods of analysed

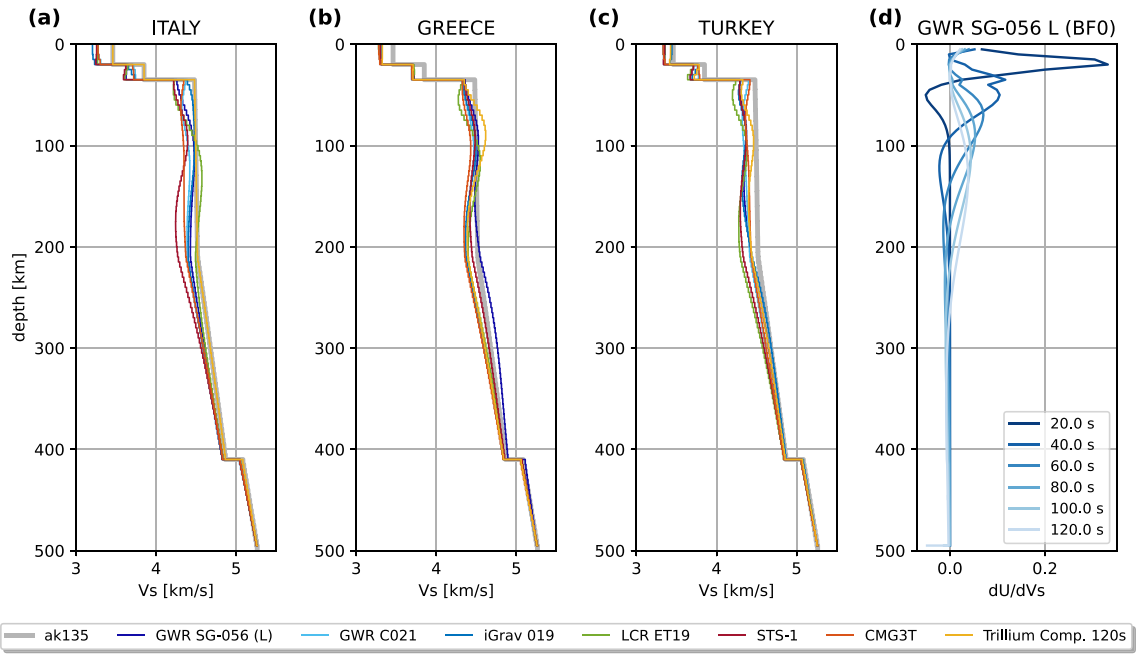

Fig. 6 Results of linear inversion method of dispersion curves of a fundamental-mode Rayleigh wave. All inverted models together with the initial ak135 model (**a**–**c**). Sensitivity kernels **d** for SG from the Black Forest station (the Greece region)

seismic waves, the sensitivity kernels are presented only for one instrument—the superconducting gravimeter GWR SG-056 L (the Greece region). It is clear that surface waves of longer periods are more sensitive to deeper structures of the Earth, but at the same time, they sample the broader depth range.

Resolution matrices

The resolution matrix relates the estimated model to the true one. Thanks to such matrix, the sensitivity of the dispersion curves to the model parameters and inversion scheme can be shown. When the true model and the estimated one are identical, the resolution matrix is the identity matrix. The system is underdetermined, so regularisation (damping and smoothness) is used to stabilise the inversion. For estimation of the changes in the model, singular value decomposition is applied. The application of the damping procedure causes a reduction of amplitudes of the resolution matrix, and the application of the smoothing procedure generates its asymmetry (Gubbins 2004).

The resolution matrices are calculated for models inverted for each instrument and region to estimate the resolution and accuracy of the inverted models. Fig. 7 shows the example of resolution matrices together with marked maximum and optimum resolution depths for the Membach station. The maximum resolution depth is estimated as a depth for which the diagonal value of the resolution matrix exceeded zero, searching from the deepest layers. The optimum resolution depth is additionally automatically estimated as the depth at which maxima of amplitude contours converged. In some cases, it is impossible to determine the optimum depth automatically, e.g. for the CMG3T (Membach seismic station) and Western Turkey region. In general, the resolution of inverted models decreases with depth (amplitudes of resolution matrix decrease). Moreover, the resolution is strongly distorted at the greater depth because of applying a smoothing procedure. Resolutions matrices with marked maximum and optimum resolution depths for all instruments and regions are presented in (Additional file 1: Fig. S2).

Maximum period of each averaged dispersion curve together with depths estimated based on sensitivity kernels (the depth at which $\frac{\delta U}{\delta V_s}$ reaches its maximum) and resolution matrices (optimum and maximum values) are summarised in Table 2. Generally, the depth estimated based on sensitivity kernels is directly proportional to the maximum period of the dispersion curve. The asymmetry in the resolution matrix causes that the values of optimum and maximum resolution depths are not linearly proportional to the maximum period of the dispersion curve. The larger the maximum period, the deeper structure can be retrieved based on the inversion procedure. Results of the linear inversion (Fig. 6) shows that all inverted models for depths larger than about 220 km converge to the starting ak135 model. The optimum resolution depth is closed to the depth estimated from a sensitivity kernels, and therefore it is later used for the estimation of final depth of V_s model.

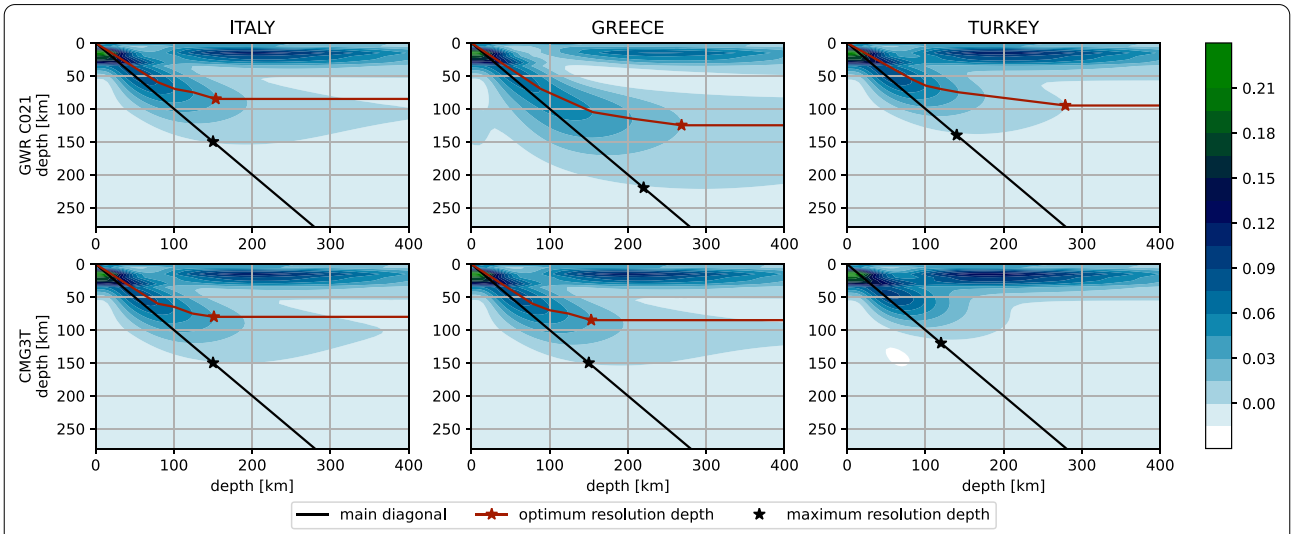

Fig. 7 Resolution matrices of the inversion scheme for the GWR C021 superconducting gravimeter and CMG3T broadband seismometer (Membach) for three regions: Italy, Greece and Western Turkey. The maximum resolution depth is marked with a black star and the optimum resolution depth with a red star

Checkerboard tests

Checkerboard tests can ensure additional insight into the data and are designated to investigate the adequacy of the initial model and the stability of the inversion scheme (Chrapkiewicz et al. 2020). The checkerboard tests can be used to test the ability of the inversion scheme to reconstruct velocity anomalies (in the presented study with depth). Positive and negative anomalies of constant thickness are added to the inversion result. The dispersion curve for the perturbed model is calculated, and the inversion algorithm is applied with the same parameters as for the unperturbed model. Later, the inverted perturbed model is subtracted from the initial perturbed model to compare the recovered with original anomalies.

The checkerboard tests are performed for sets of positive and negative anomalies of 5–150 km thicknesses, every 5 km, respectively. The amplitude of anomalies is equal to 5% of mean V_s of layers corresponding to the anomaly thickness. The reasonable reconstruction of anomalies is observed for anomaly's thickness larger than 20 km, but it is adequate only for the first 2 anomalies. In Fig. 8, the example of recovered anomalies of 20 and 60 km thicknesses for the SG of the Membach station are presented. The second wiggle is a bit out of phase with the induced pattern for anomaly thickness of 20 km, however it is still a satisfactory resolution at this depth taking into account the vertical sensitivity of surface wave in a considered period range. Additional file 1 contains results of checkerboard tests for all instruments and regions (Additional file 1: Fig. S3–S8).

Molinari et al. (2015) discouraged using the above-presented checkerboard initials and chose a random 2-D map of velocity anomalies as an input model to test the horizontal resolution of phase and group-velocity distributions of Rayleigh waves. However, it must be remembered that in the presented study, the vertical resolution of share-wave velocity distribution is tested instead of the horizontal resolution of the group-velocity of Rayleigh waves. In such a case, the proposed classical checkerboard initials seem to be the most appropriate and give an enhancement of the resolution ability of group-velocity dispersion curve with depth.

The coefficients of correlation between the original and recovered anomalies of $20-150$km thicknesses for the GWR C021 (Membach) for three regions: Italy, Greece and Western Turkey are presented in Fig. 9. The correlation coefficient (CC) is calculated as a variant of Pearson's correlation and is equivalent to cosine similarity (Manning 2008). The value of the CC between the original and recovered anomaly curves for each depth (length of correlated curves equal to the considered depth starting from the surface) and each anomaly thickness is calculated. Generally, the correlation coefficient values larger than 0.9 are observed between two uppermost original and recovered anomalies no matter what their thickness is (white dashed line in Fig. 9), which could be a simple rule of thumb for determining the resolution depth of a given anomalies. The coefficient of correlation of original and recovered anomalies for all instruments and regions are shown in the (Additional file 1: Fig. S9).

Final models

All final V_s models are presented in Fig. 10—depth ranges are estimated based on automatically determined optimum resolution depths (see Table 2). If the optimum

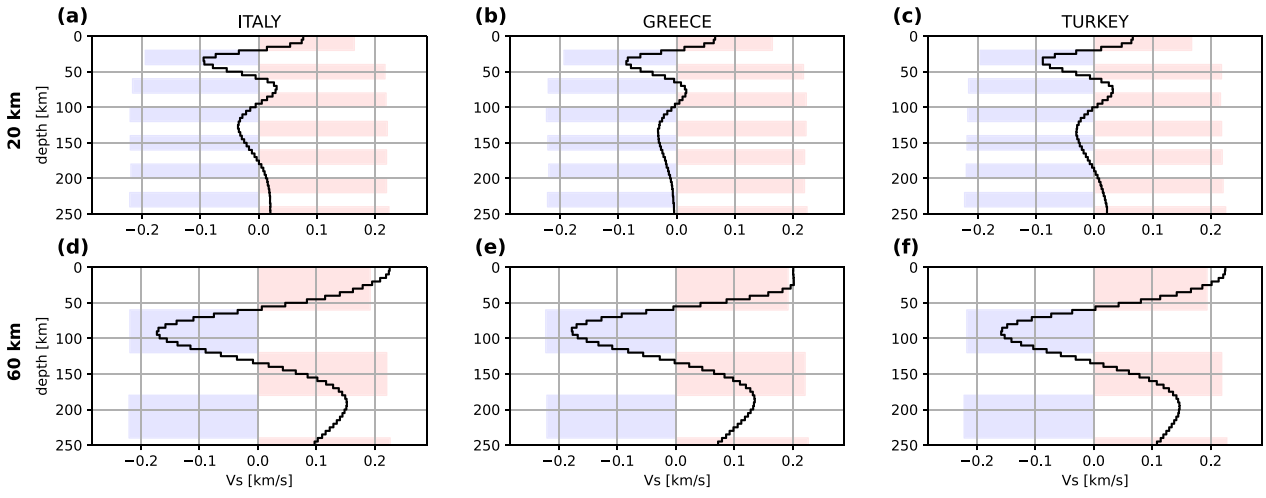

Fig. 8 Examples of checkerboard test of the inverted model for the GWR C021 superconducting gravimeter (Membach) for three regions: Italy (**a**, **d**), Greece **b**, **e** and Western Turkey (**c**, **f**); positive/negative anomalies thicknesses equal to 20km **a**–**c** and 60km **d**–**f** (red/blue shaded areas) together with recovered anomalies (black solid line)

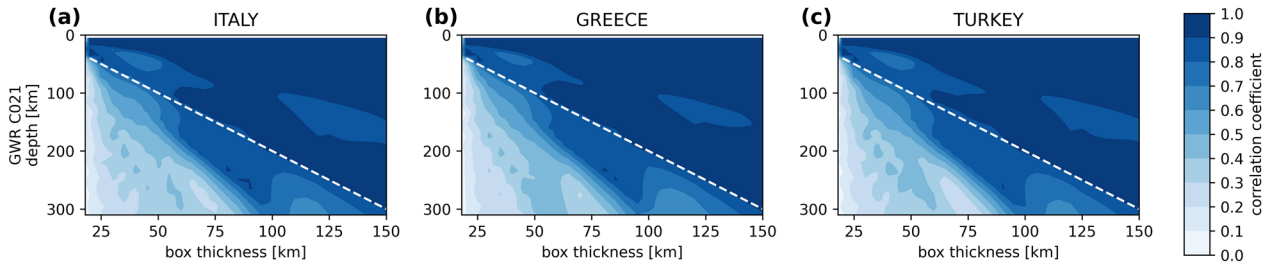

Fig. 9 The coefficient of correlation of original and recovered anomalies for the GWR C021 superconducting gravimeter (Membach) for three regions: Italy (**a**), Greece **b** and Western Turkey (**c**), respectively. The depth range of two uppermost anomalies is marked by dashed white lines

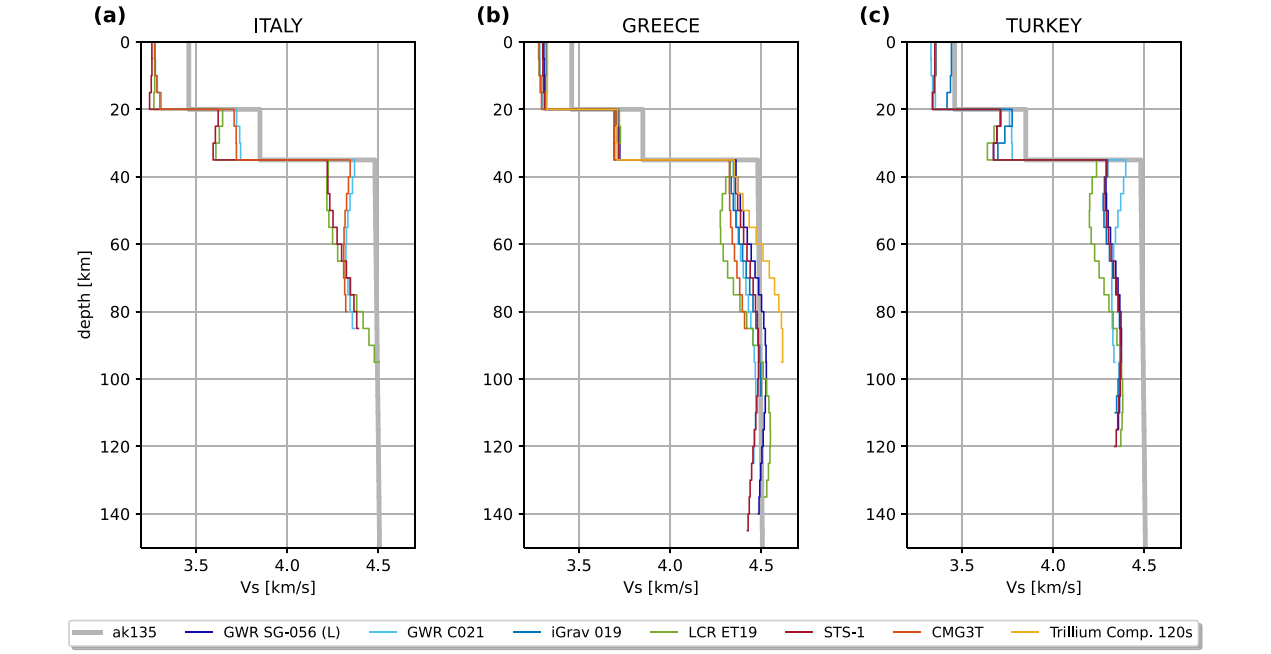

Fig. 10 Averaged distribution of S-wave velocity (V_S) with depths between instruments and earthquakes' epicentres from the Italy, Greece and Western Turkey regions

Table 2 List of instruments for all regions investigated (Italy, Greece, Western Turkey) with maximum period (T max), sensitivity kernels (sk) depth, optimum (opt) and maximum (max) resolution depths

Instrument	Italy				Greece				Turkey			
	T [s]	Depth [km]			T [s]	Depth [km]			T [s]	Depth [km]		
	Max.	Sk	Opt.	Max.	Max.	Sk	Opt.	Max.	Max.	Sk	Opt.	Max.
LCR ET19	65	75	95	130	120	140	135	240	110	125	120	200
GWR SG-056 L	55	65	–	110	120	140	140	250	100	115	115	200
STS-1	75	85	85	150	130	150	145	260	110	125	120	210
GWR C021	75	85	85	150	110	125	125	220	70	80	95	140
CMG3T	75	85	80	150	75	85	85	150	60	70	–	120
iGrav 019	50	60	–	100	90	105	105	190	95	110	110	190
Trillium Copm. 120s	–	–	–	–	60	70	95	130	55	65	–	110

resolution depth cannot be automatically determined, the final model is not shown.

The final models can be divided into three parts confirmed by the checkerboard tests: an upper crust, a lower crust, and an uppermost mantle. Models presented by, e.g. Stehly et al. (2009); Li et al. (2010); Molinari et al. (2015); Lu et al. (2018) also showed simple two layers structure of the crust of this area. What's more, because of the nature of the method, the result of linear inversion should be considered as V_s differences from the starting model rather than as an absolute V_s.

The V_s in the upper crust for all regions are relatively constant. They are lower by about 5.4, %, 4.5 %, and 3.3 % comparing to the starting ak135 model for the Italy, Greece, and Western Turkey regions, respectively. Similar relations between velocities at the depth of 20 km have been reported by Lu et al. (2018). Much larger velocities (lower by about 0.7% in relation to the ak135 model) in the upper crust observed for the iGrav 019 (SG at the Rochefort station) for the Western Turkey region are most probably not well documented because of a low number of earthquakes recordings used for the estimation of the averaged dispersion curve.

Similar features of final models are observed in the lower crust. The V_s are by 6.1 % and 3.2 % lower than in the starting ak135 model for the Italy region for the Black Forest and Membach stations, respectively. The larger velocities between the Black Forest and Membach locations at the depth of 20–35 km, comparing to the rest of the path between the Black Forest station and Italy epicentres, were reported by Molinari et al. (2015) and Lu et al. (2018). For the Greece region, velocities are consistent for all instruments and are by 3.7 % lower than in the ak135 model while for the Western Turkey region—V_s are systematically decreasing with depths and are by 1.9–5.5 % lower than in the starting model, being the result of complex structure along the ray paths (e.g. Lu et al. 2018).

In the uppermost mantle, V_s below the Moho are lower by 0.4–5.9 %, up to 4.7 % and 1.8–6.4 % compared to the starting ak135 model for Italy, Greece and Western Turkey regions, respectively. The lowest values of V_s are observed at the depths of 60–70 km and 50–65 km for the Italy and Western Turkey regions, respectively. That noticeable lowering of V_s is connected with roots of Apennines, Balkans and Alps mountains (e.g. Lu et al. 2018). For the Greece earthquakes, below the Moho depth the resulting models lose their consistency due to sampling by waves two structures with distinctly different V_s distributions with depths, i.e. the Adriatic plate and Dinarides. Also, Yang et al. (2007) reported an existence of low-velocity anomaly at the 2-D map of Rayleigh group-velocities of the period of 35 s located at the southern margin of these units causing the diffraction of surface waves and breaking the assumptions on great circles of waves propagation (Kolínský et al. 2020).

The presented final models of the crust and uppermost mantle, describing the V_s distribution down to the depth of 145 km, provide averaged information about the Earth's structure along the regional surface waves paths.

Conclusion

Data recorded by tidal gravimeters (SG and spring gravimeters), VBB and BB seismometers (only vertical component) were analysed. The period range of 10–180 s was considered to show the potential of tidal gravimeters for determining the regional Earth's structure based on intermediate-period surface wave recordings. Group-velocity dispersion curves of Rayleigh waves were measured from the recordings of earthquakes taking place in Italy, Greece, and Western Turkey. All averaged regional dispersion curves were inverted by the linear inversion method. The range of depth for which a final model was reliable as well as credibility of the observed features of the structure were determined from the qualitative analysis of the resolution matrix, sensitivity kernels, and checkerboard tests.

Presented averaged group-velocity dispersion curves of Rayleigh waves estimated based on recordings of tidal gravimeters and co-located seismometers were very consistent with each other in the period ranges of instruments' operability. Furthermore, thanks to a higher tidal gravimeters sensitivity, gravimetric data could complement BB seismic recordings for periods over 60–70 s. As a result, more good-quality recordings of regional earthquakes were available for analysis, which was especially important for regional averaging when generally a lower amount of individual measurements is available. On the other hand, it was possible to verify gravimetric recordings of earthquakes by the co-located VBB seismometer (e.g. STS-1).

The resolution depth of inverted model is closely related to maximum periods of dispersion curves and the applied inversion scheme. In this study, the reliable dispersion curves were estimated up to periods of 50-130 s, resulting in estimation of the V_s down to the depth of 80-145 km. The final models could be divided into three parts confirmed by the checkerboard tests: an upper crust, a lower crust, and an uppermost mantle.

It can be concluded that recordings of intermediate-period surface waves by tidal gravimeters, especially superconducting ones, are very reliable (high consistency between results from gravimeters and seismometers) and these instruments show the potential for using them in regional studies. This approach may be particularly advantageous for stations where very broadband seismic sensor is not available. Gravimetric data can complement

the recording of seismometers, especially those with a corner period below 120 s.

Although gravimeters show great potential for using their records in seismic surveys, it is crucial to be aware of the limitations of those instruments. First, the signal can be saturated for significant (and close) earthquakes because of the dynamic range of superconducting gravimeters. Such corrupted waveforms must be omitted when analysing surface waves. Here, the solution could be the (additionally) use of a spring gravimeter such as gPhoneX. The second limitation arises from the availability of the gravimeter's transfer function, which must be applied especially for intermediate-period analyses. Operators of gravimeters could be encouraged to perform such studies. The most valuable data from SG are in cases when the observatory is not equipped with a VBB seismometer, or its instrument has a corner period below 100 s. Overall, concerning inversion strategies, beyond the linear inversion methods, global search inversion methods such as the Monte Carlo algorithm could also be applied in further research.

Supplementary Information

The online version contains supplementary material available at https://doi.org/10.1186/s40623-022-01712-4.

Additional file 1: Figure S1 probability density distribution maps for all instruments calculated using all estimated individual dispersion curves; **Figure S2** resolutions matrices with marked maximum and optimal resolution depths for all instruments and regions; **Figures S3–S8** the checkerboard tests performed for sets of positive and negative anomalies of selected thickness for the Black Forest and Membach stations (both superconducting gravimeter and broad-band seismometer); **Figure S9** the coefficients of correlation between the original and recovered anomalies of 20–150 km thicknesses for all instruments for three regions: Italy, Greece and Western Turkey.

Acknowledgements
The ObsPy package was used for the data processing (Krischer et al. 2015). Inversion and forward procedure as well as checkerboard test, residual matrices and sensitivity kernels calculation, were performed with the use of the Computer Programs in Seismology package (Herrmann 2013). Almost all visualisations were made with the use of Matplotlib library (Hunter 2007) except geological map, which was composed in QGIS software (QGIS Development Team 2020). The authors thank two anonymous reviewers whose very constructive comments improved a lot the manuscript. The authors also wish to thank Jan Krynski for his valuable remarks.

Author contributions
K. Karkowska overall downloaded data, designed the study and performed computations. M. Wilde-Piorko provided assistance in the developing of the methodologies and applications for analysing data. Both authors read and approved the final manuscript.

Funding
This work was done within the research project No. 2017/27/B/ST10/01600 financed from the Polish National Science Centre funds.

Availability of data and materials
The facilities of IRIS Data Services, and specifically the IRIS Data Management Center, were used for access to waveforms (seismic data and gravimetric data from the Black Forest, Membach and Rochefort stations), related metadata, and/or derived products used in this study. IRIS Data Services are funded through the Seismological Facilities for the Advancement of Geoscience and EarthScope (SAGE) Proposal of the National Science Foundation under Cooperative Agreement EAR-1261681. The list of earthquakes was downloaded from the European Mediterranean Seismological Centre bulletin (https://www.emsc-csem.org/Earthquake/).

Declaration

Competing interests
The authors declare that they have no competing interests.

Author details
[1]Centre of Geodesy and Geodynamics, Institute of Geodesy and Cartography, Z. Modzelewskiego St. 27, 02-679 Warsaw, Poland. [2]Present Address: Geohazards Centre, Polish Geological Institute-National Research Institute, Rakowiecka St. 4, 00-975 Warsaw, Poland.

Received: 6 May 2022 Accepted: 25 September 2022
Published online: 10 October 2022

References

Banka D, Crossley D (1999) Noise levels of superconducting gravimeters at seismic frequencies. Geophys J Int 139(1):87–97. https://doi.org/10.1046/j.1365-246X.1999.00913.x

Bensen G, Ritzwoller M, Barmin M, Levshin A, Lin F, Moschetti M, Shapiro N, Yang Y (2007) Processing seismic ambient noise data to obtain reliable broad-band surface wave dispersion measurements. Geophys J Int 169(3):1239–1260. https://doi.org/10.1111/j.1365-246X.2007.03374.x

Bormann P, Engdahl E, Kind R (2012) Seismic wave propagation and Earth models. In: New Manual Of Seismological Observatory Practice 2 (NMSOP-2). Deutsches GeoForschungsZentrum GFZ, pp 15–27. https://doi.org/10.2312/GFZ.NMSOP-2_ch2

Van Camp M (1999) Measuring seismic normal modes with the GWR C021 superconducting gravimeter. Phys Earth Planet Inter 116(1–4):81–92. https://doi.org/10.1016/S0031-9201(99)00120-X

Van Camp M, Viron O, Watlet A, Meurers B, Francis O, Caudron C (2017) Geophysics from terrestial time-variable gravity measurements. Rev Geophys 55(4):938–992. https://doi.org/10.1002/2017RG000566

Chrapkiewicz K, Wilde-Piórko M, Polkowski M, Grad M (2020) Reliable workflow for inversion of seismic receiver function and surface wave dispersion data: a "13 BB Star" case study. J Seismol 24(1):101–120. https://doi.org/10.1007/s10950-019-09888-1

Du Z, Michelini A, Panza G (1998) EurID: a regionalized 3-D seismological model of Europe. Phys Earth Planet Inter 106(1–2):31–62. https://doi.org/10.1016/S0031-9201(97)00107-6

Dziewonski A, Bloch S, Landisman M (1969) A technique for the analysis of transient seismic signals. Bull Seismol Soc Am 59(1):427–444. https://doi.org/10.1785/BSSA0590010427

Forbriger T, Zuern W, Widmer-Schnidrig R (2021) Challenges and perspectives for lowering the vertical-component long-period detection level. Seismol Res Lett 92(4):2498–2512. https://doi.org/10.1785/0220200399

Freybourger M, Hinderer J, Trampert J (1997) Comparative study of superconducting gravimeters and broadband seismometers STS-1 / Z in seismic and subseismic frequency bands. Phys Earth Planet Inter 101(3–4):203–217. https://doi.org/10.1016/S0031-9201(97)00003-4

Gubbins D (2004) The under-determined problem. Time series analysis and inverse theory for geophysicists. Cambridge University Press, Cambridge, pp 110–124

Herrmann R (2013) Computer programs in seismology: an evolving tool for instruction and research. Seismol Res Lett 84(6):1081–1088. https://doi.org/10.1785/0220110096

Herrmann R, Ammon C (2004) Surface waves, receiver functions and crustal structure, Computer Programs in seismology: version 3.30. Saint Louis University

Hunter J (2007) Matplotlib: a 2D graphics environment. Comput Sci Eng 9(03):90–95. https://doi.org/10.1109/MCSE.2007.55

Karkowska K, Wilde-Piórko M, Dykowski P (2022) Analysis of earthquakes recordings of tidal gravimeters in the period range of 10–1000 s. Acta Geodyn Geomater 19(1):79–92. https://doi.org/10.13168/AGG.2021.0043
Kennett B, Engdahl E, Buland R (1995) Constraints on seismic velocities in the Earth from traveltimes. Geophys J Int 122(1):108–124. https://doi.org/10.1111/j.1365-246X.1995.tb03540.x
Kolínský P (2004) Surface waves dispersion curves of Eurasian earthquakes: the SVAL program. Acta Geodyn Geomater 1(2):165–185
Kolínský P, Schneider F, Bokelmann G (2020) Surface wave diffraction pattern recorded on AlpArray: cameroon volcanic line case study. J Geophys Res Solid Earth 125. https://doi.org/10.1029/2019JB019102
Krischer L, Megies T, Barsch R, Beyreuther M, Lecocq T, Caudron C, Wassermann J (2015) ObsPy: a bridge for seismology into the scientific Python ecosystem. Comput Sci Discov 8. https://doi.org/10.1088/1749-4699/8/1/014003
Lander AV (1989) Frequency-time analysis. In: Keilis-Borok VI (ed) Seismic surface waves in a laterally inhomogeneous earth. Kluwer Academic Publishers, Dordrecht, pp 153–163
Levshin A, Yanovskaya T, Lander A, Bukchin B, Barmin M, Ratnikova L, Its E (1989) Recording, identification, and measurement of surface wave parameters. In: Keilis-Borok VI (ed) Seismic surface waves in a laterally inhomogeneous earth. Kluwer Academic Publishers, Dordrecht, pp 131–182
Li H, Bernardi F, Michelini A (2010) Surface wave dispersion measurements from ambient seismic noise analysis in Italy. Geophys J Int 180(3):1242–1252. https://doi.org/10.1111/j.1365-246X.2009.04476.x
Li H, Xu J, Chen X, Sun H, Zhang M, Zhang L (2020) Extracting long-period surface waves and free oscillations using ambient noise recorded by Global Distributed Superconducting Gravimeters. Seismol Res Lett 91(4):2234–2246. https://doi.org/10.1785/0220190166
Lu Y, Stehly L, Paul A, AlpArray Working Group (2018) High-resolution surface wave tomography of the European crust and uppermost mantle from ambient seismic noise. Geophys J Int 214(2):1136–1150. https://doi.org/10.1093/gji/ggy188
Manning C, Raghavan P, Schütze H (2008) The vector space model for scoring. Introduction to information retrieval. Cambridge University Press, Cambridge, pp 110–116
Molinari I, Verbeke J, Boschi L, Kissling E, Morelli A (2015) Italian and Alpine three-dimensional crustal structure imaged by ambient-noise surface-wave dispersion. Geochem Geophys Geosyst 16(12):4405–4421. https://doi.org/10.1002/2015GC006176
Pawlewicz M, Steinshouer D, Gautier D (2002) Map showing geology, oil and gas fields, and geologic provinces of Europe including Turkey. U.S. Geological Survey. https://doi.org/10.3133/ofr97470I
QGIS Development Team (2020) QGIS geographic information system. Open source geospatial foundation. http://qgis.org
Richter B, Wenzel H, Zürn W, Klopping F (1995) From Chandler wobble to free oscillations: comparison of cryogenic gravimeters and other instruments in a wide period range. Phys Earth Planet Inter 91(1–3):131–148. https://doi.org/10.1016/0031-9201(95)03041-T
Ritzwoller M, Levshin A (1998) Eurasian surface wave tomography: group velocities. J Geophys Res Solid Earth 103(B3):4839–4878. https://doi.org/10.1029/97JB02622
Romanowicz B (2002) Inversion of surface waves: a review. In: Lee W (ed) International handbook of earthquake and engineering seismology. Academic Press, Part A, Cambridge, pp 149–173
Rosat S, Hinderer J, Crossley D, Boy J (2004) Performance of superconducting gravimeters from long-period seismology to tides. J Geodyn 38(3–5):461–476. https://doi.org/10.1016/j.jog.2004.07.005
Rosat S, Sato T, Imanishi Y, Hinderer J, Tamura Y, McQueen H, Ohashi M (2005) High-resolution analysis of the gravest seismic normal modes after the 2004 Mw = 9 Sumatra earthquake using superconducting gravimeter data. Geophys Res Lett 32. https://doi.org/10.1029/2005GL023128
Soomro R, Weidle C, Cristiano L, Lebedev S, Meier T, PASSEQ Working Group (2016) Phase velocities of Rayleigh and Love waves in central and northern Europe from automated, broad-band, interstation measurements. Geophys J Int 204(1):517–534. https://doi.org/10.1093/gji/ggv462
Stehly L, Fry B, Campillo M, Shapiro N, Guilbert J, Boschi L, Giardini D (2009) Tomography of the Alpine region from observations of seismic ambient noise. Geophys J Int 178(1):338–350. https://doi.org/10.1111/j.1365-246X.2009.04132.x
Verbeke J, Boschi L, Stehly L, Kissling E, Michelini A (2012) High-resolution Rayleigh-wave velocity maps of Central Europe from a dense ambient-noise data set. Geophys J Int 188(3):1173–1187. https://doi.org/10.1111/j.1365-246X.2011.05308.x
Yang Y, Ritzwoller M, Levshin A, Shapiro N (2007) Ambient noise Rayleigh wave tomography across Europe. Geophys J Int 168(1):259–274. https://doi.org/10.1111/j.1365-246X.2006.03203.x

Publisher's Note